Macromolecules

pubs.acs.org/Macromolecules Article

Adaptable Networks with Semiorthogonal Two-Stage Polymerizations Enabled by Sequential Photoinitiated Thiol−Ene and Disulfide−Ene Reactions

Yunfeng Hu, Shafer M. Soars, Bruce E. Kirkpatrick, Maciej Podgorski, Nicholas Bongiardina, Benjamin D. Fairbanks, Kristi S. Anseth, and Christopher N. Bowman*

Cite This: *Macromolecules* 2023, 56, 9778−9786 Read Online

ACCESS | Metrics & More | Article Recommendations

ABSTRACT: Sequential thiol−ene and disulfide−ene photopolymerizations and their utility in materials applications such as shape fixation, photolithography, and holographic recording were explored. Though thiol−ene and disulfide−ene reactions are both radical-mediated and share a common reactive group, the fact that they have several orders of magnitude difference in the reaction rate was utilized to form two-stage photopolymers with high specificity in a sequential and semiorthogonal manner. While the faster thiol−ene reaction was utilized to form a first-stage matrix, the disulfide−ene reaction was then initiated to break cross-links via disulfide cleavage and subsequently form twice as many thioether bonds as new cross-links. As such, sequential bond breakage and formation, enabling the dynamic behavior in the second stage of a single network, were explored and applied in various scenarios. Combining a remarkable difference in mechanical properties between the two stages, the dynamic photopolymer materials were capable of enabling shape fixation by initiating the second-stage polymerization while being strained and deformed. Photolithography was then utilized to quantify shape retention in deformed samples, revealing a fidelity of approximately 95% following the second-stage cure. Additionally, polarized light microscopy was used to understand better how these mechanisms affect the mechanical properties of the material when stress is applied. Finally, taking advantage of the integrated network in the two-stage system, the photopolymers were employed to record a holographic grating with a refractive index modulation (Δn) of 0.0022 and functionally nearly zero haze.

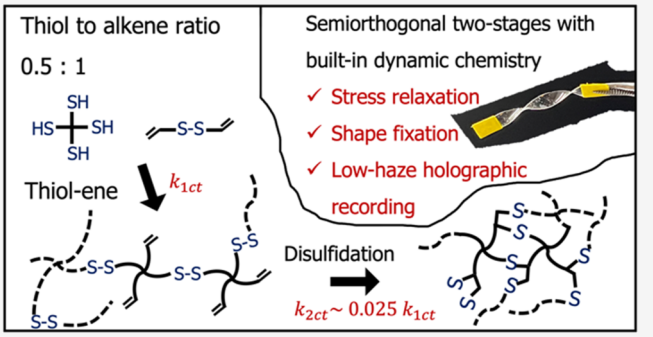

INTRODUCTION

For more than 50 years, the vast utility of photopolymers has been demonstrated in a variety of fields, including materials science, optics, and medicine.[1−5] The remarkable impact of these materials is, in part, from these systems possessing uniquely efficient and selective spatiotemporal control over reactions achieved by light-initiated chemistries,[6,7] as well as relatively low-toxicity solvent and catalyst requirements.[8,9] Two-stage systems are of particular interest among photopolymer formulations for their programmability and novel applications enabled by sequential curing steps, which allow for user-defined variability in local mechanical and optical properties through patterned illumination.[10,11]

Two-stage photopolymer systems incorporate two or more orthogonal or semiorthogonal chemistries, allowing for two (or multi)-stage, sequential polymerizations of separate monomers, during which at least one stage (usually the second stage) is photopolymerized. These materials have broad applications in shape fixation,[12,13] photolithography,[14] and holography.[15] Shape fixation in two-stage materials is usually achieved in second-stage polymerization when deformations in the first-stage network are stabilized mechanically.[16] Similarly, two-stage photopolymers offer unique advantages for lithography, for example, nanoimprint lithography, in which resists require differing material properties in the imprinting step (soft enough to deform) and the final material properties (stiff and durable).[17,18] Beyond mechanical property programming, spatial patterning of the refractive index is often utilized in two-stage systems for applications such as holographic gratings.[19] However, in these applications, two-stage polymer formulations suffer from several limitations, including phase separation and unwanted diffusion of mobile species during the reaction, leading to haze and limited transparency in optical

Received: August 28, 2023
Revised: November 10, 2023
Accepted: November 15, 2023
Published: November 29, 2023

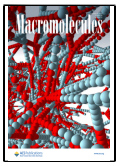

Scheme 1. (a) Thiol−Ene Reaction. (b) Disulfidation of Vinyl Ethers. (c) Monomers Used in This Study

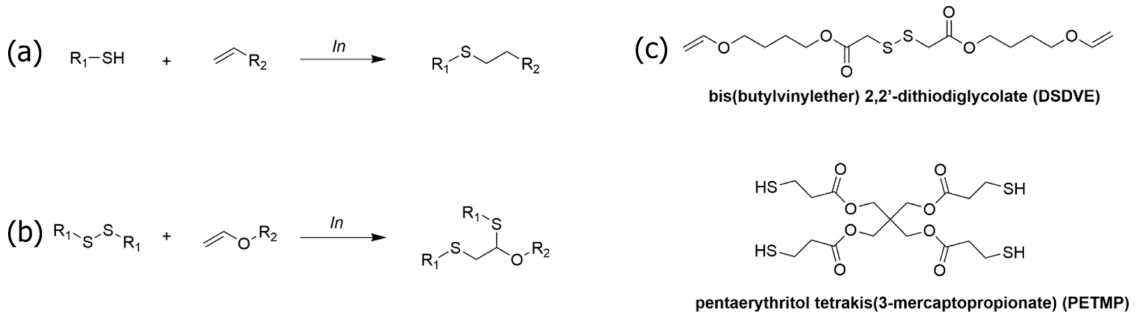

Scheme 2. Mechanism of the Competing Thiol−Ene and Disulfide−Ene Reactions with a Vinyl Ether[a]

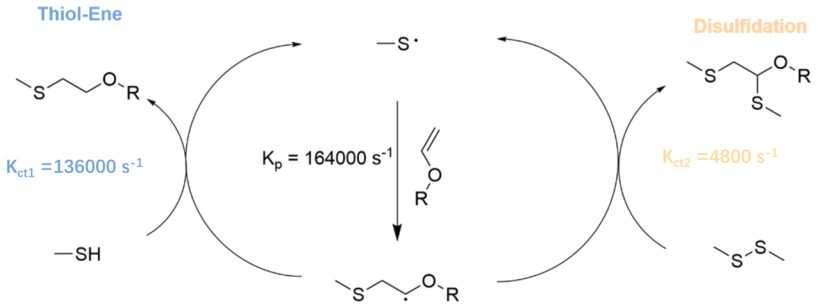

[a]Chain transfer constants (K_{ct1}/K_{ct2}) indicate that the thiol−ene reaction is approximately 30 times faster than the disulfidation reaction.

materials and diminishing the fidelity of patterning or shape programming.[20−23]

To mitigate the aforementioned challenges, the formation of covalent bonds between the monomer components involved in both curing steps has proven to be extremely valuable for improving the fidelity of second-stage photopolymerizations. Covalent attachment facilitates increased similarity between the chemical species in each curing stage and decreases mobility, thus limiting phase separation thermodynamically and kinetically. Furthermore, covalent attachment between mobile species and relatively immobile first-stage polymers significantly reduces unwanted diffusion and blurring effects on final patterns.[24] Distinctive reaction and material strategies are often required to achieve efficient covalent attachment during second-stage polymerization. For example, functional groups that readily react with monomers in the second-stage polymerization are incorporated into the first-stage polymers to facilitate attachment between the two stages. However, the benefit of such covalent attachment largely depends on the reaction rate of those introduced functionalities,[25] as slow attachment formation might still allow enough time for phase separation and unwanted diffusion to occur. Theoretically, the incorporation of reactive monomers for second-stage polymerization into the first-stage polymer would enable the efficient and rapid formation of covalent attachment between two stages, during which mobile species are prohibited from diffusion and rearrangement. To design such two-stage systems, proper selection of reaction and monomer chemistries is necessary.

Recently, our group reported a photomediated disulfidation reaction that is both kinetically semiorthogonal to the thiol−ene reaction (Scheme 1a) and comparatively adds twice the number of sulfur atoms to an alkene (Scheme 1b).[26] The semiorthogonality of these reactions is apparent based on the drastic differences in the polymerization rate between the two competing reactions. This disulfidation reaction is an attractive means to obtain useful materials with high sulfur content and 100% atom economy, marking it as complementary to thiol−ene cross-linking for two-stage networks with sequential changes in mechanical properties and refractive index, which can be spatiotemporally controlled by light initiation. Furthermore, two-stage materials containing disulfides in the backbone of their initial network are able to relax stress to some degree during the second-stage polymerization.[27,28] The stress relaxation during the second stage is beneficial for more efficient second-stage hologram formation and more homogeneous final networks when compared to typical two-stage systems without such dynamic properties.[29,30]

In this work, dynamic two-stage photopolymer systems are demonstrated utilizing monomers compatible with both thiol−ene and disulfide−ene chemistries (Scheme 1c) to enable applications in reshapable materials, lithography, and holography. The semiorthogonality of these reactions imparted by their relative reaction rates enables the user to sequentially and spatiotemporally initiate first-stage thiol−ene cross-linking followed by second-stage disulfidation. The initial thiol−ene photopolymerization results in complete consumption of thiols and relatively low conversion of disulfides via the disulfide−ene reaction, after which most monomers are covalently attached to the first-stage network. The subsequent second-stage irradiation results in the conversion of the remaining disulfides and alkenes, conferring changes in the mechanical, chemical, and optical properties in exposed areas. Specifically, a first-stage thiol−ene matrix was strained and then fixed in its deformed shape by second-stage disulfidation, which led to a 100-fold increase in storage modulus (10 kPa to 1 MPa). This shape fixation capability was further investigated by prestraining first-stage matrices prior to second-stage spatially selective photocross-linking, illustrating potential applications for these materials as lithographic resists. Finally, the second-stage

https://doi.org/10.1021/acs.macromol.3c01728
Macromolecules 2023, 56, 9778−9786

Scheme 3. Graphical Representation of a Two-Component, Two-Stage Photopolymer System[a]

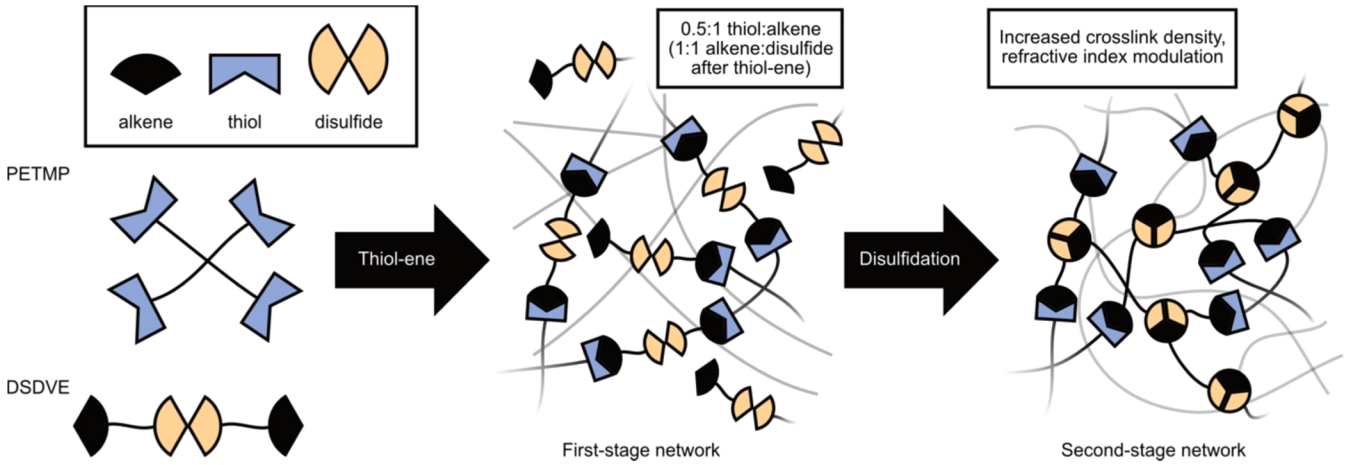

[a]Due to kinetic semiorthogonality between thiol−ene and disulfidation reactions, sequential photocuring steps yield increased storage modulus and refractive index modulation between first- and second-stage networks.

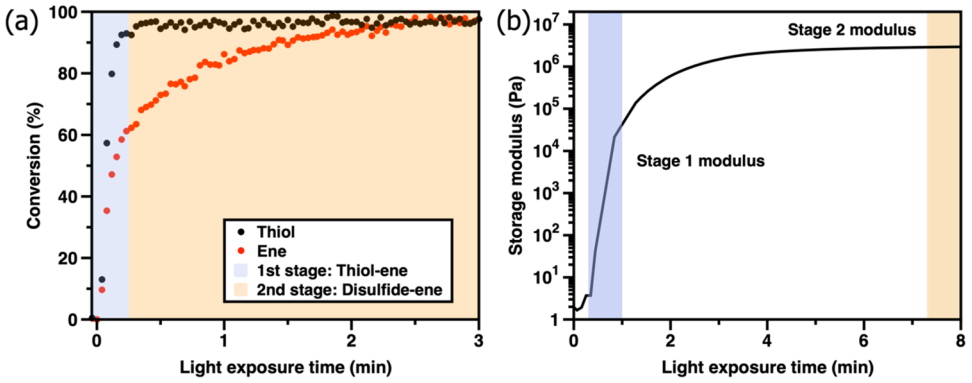

Figure 1. Two stages exhibited reaction conversion and storage modulus change. (a) Near IR demonstrating conversion over time for the thiol (PETMP) and alkene (DSDVE). The sample comprised of 0.5:1 stoichiometric equivalence of thiol/alkene with 3 wt % TPO irradiated at 405 nm at ∼10 mW/cm^2 between glass plates with 100 μm spacers. Complete conversion of the thiol is seen after roughly 15 s of exposure. (b) Shear storage modulus obtained via oscillatory rheology using a mixture of 0.5:1 stoichiometric equivalence of thiol/alkene with 3 wt % TPO irradiated at 405 nm at ∼10 mW/cm^2.

disulfidation was used to induce a spatial variation of the refractive index and generate holographic gratings with essentially no haze. These materials represent a new approach for versatile two-stage photopolymer networks that avoid the diminished performance associated with monomer phase separation and diffusion.

RESULTS AND DISCUSSION

As detailed in previous studies, radical-mediated disulfidation of vinyl ethers proceeds with 100% atom economy and overall pseudo-first-order kinetics with respect to the disulfide.[26] It was found that the rates and overall conversions of the reaction were highly dependent on the identity of the disulfide, where strong electron-withdrawing groups flanking the disulfide resulted in the fastest rates and highest overall conversions. It was shown that the thiol−ene reaction is approximately 30 times faster than the disulfide−ene reaction, demonstrating that the two functional groups react semiorthogonally (Scheme 2).

The disulfide monomer DSDVE was designed with a few key considerations in mind: the esters flanking the disulfides increase the reaction rate and overall conversions of the disulfide−ene reaction, the butyl short chains enable the miscibility of the monomer with a multifunctional thiol (tetramercaptopropionate) for cross-linking, and the vinyl ethers enable this single monomer to participate in both the stage I thiol−ene and stage II disulfide−ene reactions, thus simplifying the two-stage system to only two components (Scheme 3).

Real-time infrared spectroscopy was used to demonstrate the sequential nature of the two competing reactions and to determine the conversion of the alkene at various exposure times. A mixture of DSDVE and PETMP (0.5:1 stoichiometric equivalence of thiol/alkene) with a 3 wt % TPO photoinitiator was irradiated with 405 nm light at 10 mW/cm^2 between glass slides with 100 μm spacers (Figure 1a). At this stoichiometric ratio, complete thiol consumption results in a 50% conversion of the alkenes, leaving the remaining alkenes to react with the disulfides. Indeed, complete consumption of thiol occurred after approximately 15 s of irradiation, with roughly 40% of the alkenes unreacted. The deviation from the 50% conversion of alkenes, which would otherwise be expected in a conventional, purely orthogonal two-stage system, is primarily attributed to the slow yet simultaneous disulfidation that also occurs in the first-stage thiol−ene polymerization (i.e., semiorthogonality). Subsequently, the remaining double bonds participated in a

https://doi.org/10.1021/acs.macromol.3c01728
Macromolecules 2023, 56, 9778−9786

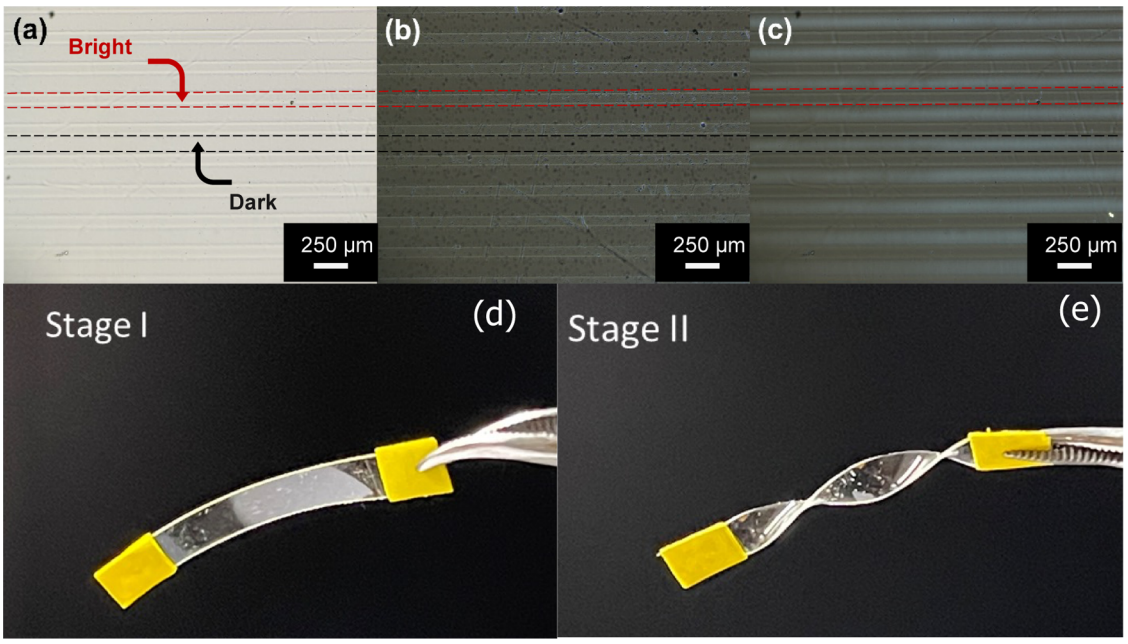

Figure 2. Study of shape fixation and mechanical response of the polymer network under strain. All formulations consisted of DSDVE and PETMP (thiol/alkene = 0.5:1) and 3 wt % TPO. Figures (a–c) are images of photolithographic patterns taken from an optical microscope. In all three figures, the same films as figure (a) were exposed to a photomask of 100/150 μm features (exposed fringes were 100 μm and unexposed fringes were 150 μm) while being either stretched with 18% strain or not. In each case, the second-stage curing was photoinitiated at an intensity of 10 mW/cm^2 for 3 min. (a) Image of features recorded in the film with 18% strain during second-stage curing using nonpolarized light. (b) Image of features recorded in the film without stretch during second-stage curing using polarized light. Stress is seen in the bright fringes. (c) Image of features recorded in the film with 18% strain during second-stage curing using polarized light. Stress is seen in dark fringes. (d) DSDVE-PETMP film sample made with 250 μm spacers after first-stage flood curing. The curing was conducted using 405 nm light for 30 s at an intensity of 10 mW/cm^2. (e) The deformation of the first-stage film was locked by a second-stage flood curing. The second-stage photopolymerization was accomplished by irradiating the sample at 405 nm at an intensity of 10 mW/cm^2 for 2 min.

slow reaction, exclusively with disulfides, as depicted in Figure 1a. After nearly 3 min of the disulfide–ene reaction, the double bond consumption approached 100%, indicating a nearly complete addition of disulfides to the double bonds. Leveraging the difference in rate between the thiol–ene and disulfide–ene reactions, these chemistries are initiated sequentially to gain selective control over the properties of the network based on the light dose. As previously demonstrated, the mechanical properties of stage 1 (G' = 10 kPa) and stage 2 (G' = 1 MPa) networks vary by approximately 100-fold (Figure 1b).[26]

Throughout the aforementioned experiments, the shelf stability of the DSDVE–thiol mixture was primarily constrained by the rapid thiol–vinyl reaction, which is significantly faster than the disulfide–ene reaction. When stored at −4 °C in the dark, the mixture displayed no discernible self-initiated polymerization. Therefore, we would not anticipate any significant stability concerns arising from the introduction of the disulfide.

Photolithography was utilized to examine how these two-stage mechanisms affect the mechanical properties of the material when strain is applied. An initial first-stage film was prepared by flood curing (405 nm, 10 mW/cm^2, 40 s) a mixture of DSDVE and PETMP (0.5:1 thiol/alkene stoichiometric ratio) with 3 wt % TPO between glass plates with 250 μm spacers. The flood-cured film was then exposed through a photomask consisting of 100 μm lines permitting light (bright fringes) spaced 150 μm apart with regions blocking light (dark fringes). During second-stage curing, these films were exposed through a photomask either directly or while being strained 18% (Figure 2a–c). These films were subsequently imaged through a cross-polarized microscope to visualize internal stresses, which are typically seen as brighter areas due to stress-induced birefringence. The films that were not stretched (Figure 2b) exhibited minor stress in bright fringes, which likely resulted from additional cross-links formed during the second-stage disulfide–ene reaction. In the films strained 18% (Figure 2c), different stress patterns were observed after second-stage photomask exposure, with birefringence in dark fringes, while bright fringes had minimal birefringence. This phenomenon is mainly attributed to the cleavage of disulfide bonds to form new thioether bonds from disulfidation reactions in the second stage, which effectively erases the applied stress and anisotropic polymer orientation in the bright fringes, which was induced in the first-stage network upon stretching. Meanwhile, the second-stage cure, which occurred in the bright fringes, led to the retention of the stretched shape across the entire sample (less than 5% reduction in pattern length following illumination and removal of the stretching apparatus), thus maintaining dark fringes in a state of high stress and polymer alignment. Overall, the different stress responses in this system, compared to conventional two-stage systems, demonstrate its distinctive dynamic character during the second-stage exposure with potential applications in the area of shape alteration/fixation.

Shape fixation in two-stage polymers is achieved via the second-stage polymerization, during which the cross-linking density and storage modulus increase dramatically. The capability of shape fixation is largely determined by the magnitude of the modulus increase in second-stage polymer-

https://doi.org/10.1021/acs.macromol.3c01728
Macromolecules 2023, 56, 9778–9786

ization, and it directly relates to the choice of second-stage chemistry and the loading of second-stage monomers. On the other hand, stress from deformation and shrinkage from secondary cross-linking diminish the shape fixation capability. Therefore, stress relaxation during second-stage polymerization is often another desirable property for high-fidelity shape fixation to avoid significant internal stresses following second-stage curing. During the second-stage disulfide−ene reaction, every disulfide moiety reacts with a double bond to form two additional thioether cross-links. Meanwhile, the cleavage of disulfide bonds accompanying the disulfide−ene addition relieves the deformation stress.[27] As such, the thiol−ene disulfidation system described herein is a perfect match for these requirements. As with the photolithography experiments, the first-stage thiol−ene photopolymerization of DSDVE and PETMP generated a transparent elastomeric film (Figure 2d). The elastomeric nature of the material allowed for geometric deformation, which was permanently locked by initiating second-stage curing of the deformed polymer (Figure 2e). The freestanding film maintained its deformed shape after the second-stage reaction, suggesting potential applications in various areas, including biomedical device development and additive manufacturing.[31]

Due to the fact that numerous thioether bonds are formed during the second-stage exposure, it was expected that this material could also have utility in optical applications as holographic photopolymers where spatial control of the refractive index is necessary.[32] Therefore, the refractive index change in each step was evaluated by using a refractometer. To be noted, given the minimal impact of 3 wt % photoinitiator loading on the refractive indices of the mixtures (i.e., approximately 0.001), we have omitted the contribution from the photoinitiator in subsequent discussions. As shown in Figure 3, the change in refractive index (Δn) between the first- and second-stage films was 0.013, which was lower than the change in refractive index between the monomer resin and first-stage films (i.e., 0.019). This increase was probably caused by disulfide cleavage in the second-stage reaction that led to the formation of two new thioether bonds. The refractive index difference between the first and second stages is directly related to the theoretical maximum refractive index modulation. In this system, assuming a perfect sinusoidal refractive index profile formed during holographic recording, the theoretical maximum would be half of 0.013, i.e., 0.0065. While this value may not be particularly high when compared to commercial holographic photopolymers, where matrix and photopolymers are formulated deliberately as chemically distinct compounds, a refractive index difference of 0.013 remains significant in the realm of holographic applications.[33] This difference is especially compelling when considering the fact that the recording medium consists solely of a cross-linked polymer network.

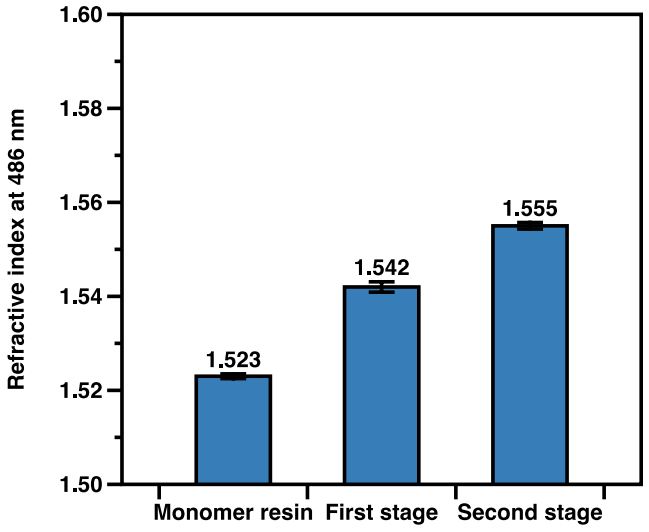

Figure 3. Refractive index values of materials. The material consisted of PETMP and DSDVE (0.5:1 thiol/alkene stoichiometric ratio) with 3 wt % TPO. The sample was cast between glass plates with 250 μm spacers and was irradiated at 405 nm at 10 mW/cm^2 for 40 s for the first-stage cure and an additional 3 min for the second-stage cure. RI values were taken of the monomer resin, post first-stage cure, and post second-stage cure.

After the first-stage thiol−ene polymerization, the cross-linked network containing both disulfides and unreacted alkenes can be used directly for holographic recording, during which the recording medium is exposed to the light intensity pattern generated by two-beam interference. Compared to conventional two-stage holographic photopolymers, in which writing monomers are fully untethered and diffuse freely during the recording, this system has minimal diffusion of untethered writing monomers (i.e., disulfides and vinyl groups) and generates a refractive index contrast between bright and dark fringes mainly by forming high-refractive-index thioether linkages from the disulfide−ene reaction and moving of tethered monomers in the dynamic network via disulfidation. Therefore, upon flood curing, recorded holographic gratings would be fully erased, as the dynamic network is activated to relieve the previous concentration profile, while the remaining disulfides and vinyl groups react and increase the refractive index in the dark fringes. As shown in Figure 4a, a clean and well-fitted angular playback curve was obtained in this system, but flood curing after recording could erase the grating completely.

The semiorthogonality between the two stages in this system is achieved by controlling the light dose in each stage of curing. Therefore, the first-stage exposure time might have a significant impact on the final refractive index contrast of holographic gratings. The first-stage curing time was varied, while a constant intensity of 10 mW/cm^2 was maintained to optimize the final refractive index modulation (Figure 4b). The optimal first-stage curing time was found to be roughly 40 s, which interestingly accounts for roughly a 75% conversion of alkenes, as depicted from the IR experiments conducted in Figure 1. This conversion of alkenes reflects complete consumption of thiol due to thiol−ene cross-linking chemistries and roughly 50% consumption of disulfides due to the disulfide−ene reaction. In this case, after the first stage, nearly all functional groups capable of reacting during the second-stage writing process are tethered to the initial matrix, minimizing any potential escape of monomers and radicals. The escape of radicals and reactive oligomers would otherwise be severe in this system due to the dynamic nature of disulfide bonds and their scission during the second-stage disulfide−ene reaction. For example, when curing times were less than 40 s, the number of untethered reactive mobile species might be significantly increased and could possibly diffuse away from the exposed area during the holographic recording, thus reducing the final refractive index contrast. Conversely, when an exposure time of more than 40 s was employed during the

https://doi.org/10.1021/acs.macromol.3c01728
Macromolecules 2023, 56, 9778−9786

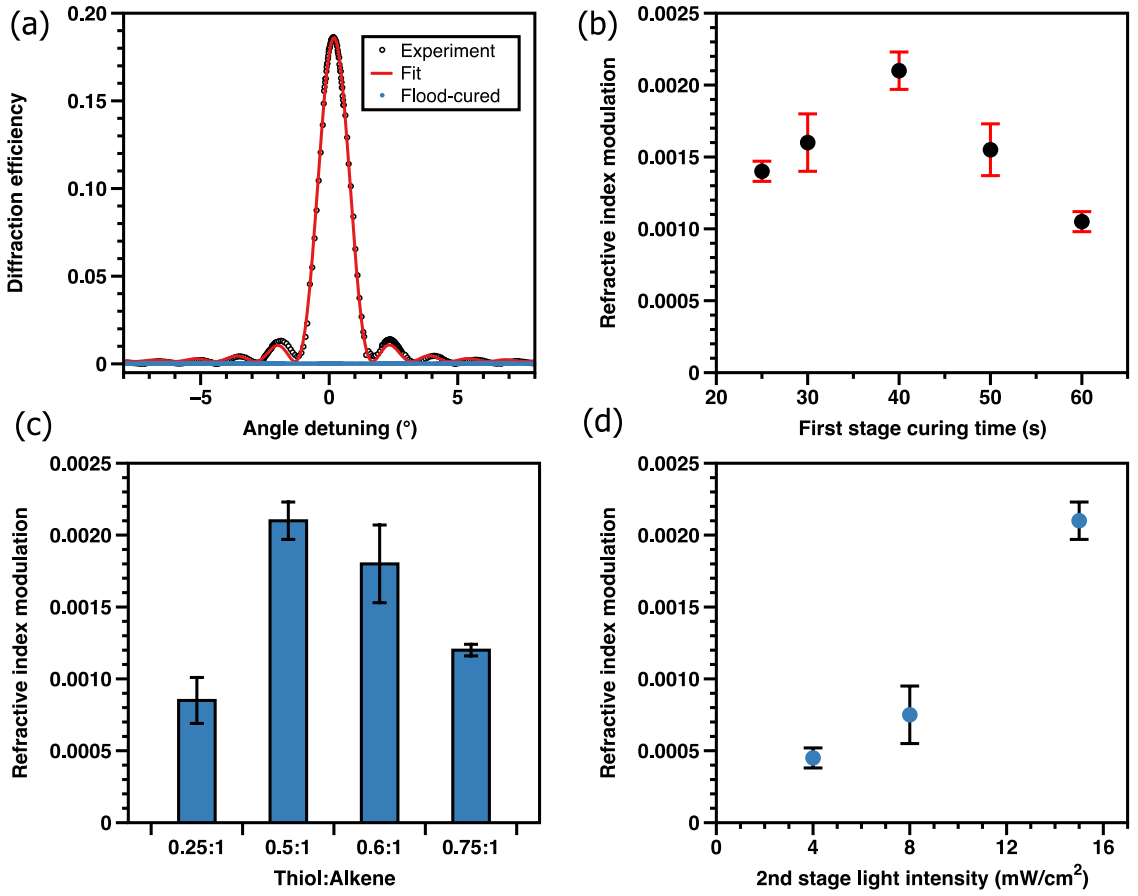

Figure 4. (a) Stage 2 diffraction efficiency plots as a function of Bragg angular detuning (degree), demonstrating good fidelity of the gratings. The gratings were formed from a stoichiometric mixture of the 0.5:1 thiol/alkene functional group ratio (using PETMP and DSDVE) with 3 wt % TPO between glass plates with a 50 μm spacer. The first-stage cure was 40 s at 10 mW/cm^2 with 405 nm light. The writing stage was achieved with a laser beam of an average intensity of 14 mW/cm^2 for 25 s. The reading beam wavelength was 633 nm. The blue curve is the playback read at the same spot after flood curing. (b) Stage 2 change in the refractive index as a function of stage 1 cure times. All conditions are identical to (a) with the exception of stage 1 cure time. (c) Stage 2 change in refractive index as a function of stoichiometric ratio between thiol and alkene. All conditions were identical to (a), with the exception of functional group equivalence. (d) Stage 2 change in refractive index as a function of intensity of light for the stage 2 writing phase. All conditions are identical to (a) with the exception of intensity of light for the 2nd stage writing cure.

first stage, too few disulfides remained to achieve high index change during the second-stage reaction.

The ratio of thiol to alkene (PETMP/DSDVE) was also varied to study its impact on the final refractive index contrast. Four different stoichiometric formulations were tested: 0.25:1, 0.5:1, 0.6:1, and 0.75:1 functional group ratios of thiol/alkene; the ratio of disulfide (which also reacts with alkenes) remained fixed at half of the vinyl ethers present. In all four formulations, 40 s of first-stage cure was used at a constant light intensity of 10 mW/cm^2, as 40 s initial cure allowed for completion of the thiol−ene reaction for each formulation while leaving a significant portion of disulfides available for subsequent second-stage cure. As expected, the 0.5:1 formulation exhibited the highest performance in Figure 4c, since this formulation facilitated optimal tethering of the writing monomer to the matrix while leaving sufficient unreacted alkenes available for the disulfide−ene writing stage. With 40 s of curing, formulations containing more thiol (0.6:1) and (0.75:1) likely have insufficient alkene concentrations for the second-stage recording of high contrast, whereas the low thiol formulation (0.25:1) has significant untethered monomer content, giving rise to severe diffusional blurring.[24]

An additional variable used for optimization was the intensity of the second-stage writing cure (Figure 4d), which showed that higher light intensities resulted in a larger change in the refractive index over this range of available light intensities. This result was probably caused by slower reaction rates of the disulfide−ene reaction at lower light intensities. Disulfides undergo radical-mediated reversible exchange, which significantly facilitates the network rearrangement during the second-stage holographic recording. A decreased disulfide−ene reaction rate enables a wider time window for network rearrangement to blur a concentration gradient and thus attenuate index contrast formed between bright and dark fringes.

High-performance holographic photopolymers are crucial for emerging holographic applications such as holographic optical elements (HOEs), which are promising solutions for developing next-generation augmented reality (AR) devices.[34] In those applications, high optical clarities of holographic gratings recorded in photopolymers are often necessary. However, controlling the phase separation of photopolymers, which induces significant unwanted light scattering (i.e., high haze and low optical clarity), remains challenging. Here, taking advantage of having most (if not all) reactive moieties for

https://doi.org/10.1021/acs.macromol.3c01728
Macromolecules 2023, 56, 9778−9786

second-stage disulfide−ene reaction tethered in the first-stage thiol−ene cross-linked network, this semiorthogonal thiol−ene and disulfide−ene system was utilized as holographic recording media to achieve high optical clarity with low haze.

The haze of final holographic gratings and first-stage films was measured (Figure 5) using a haze meter. As can be seen in

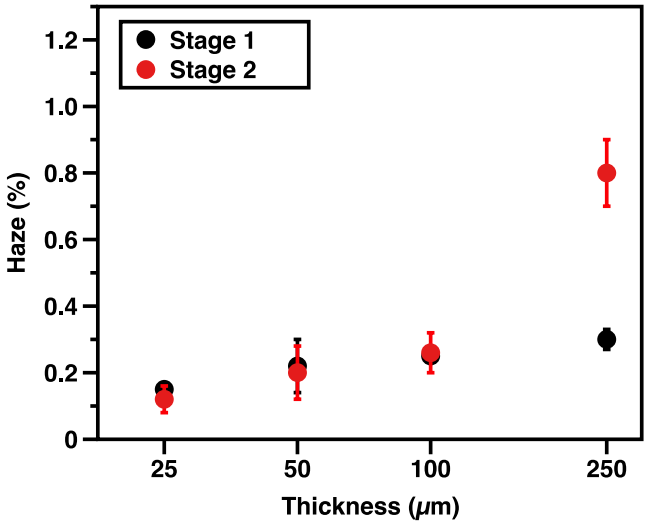

Figure 5. Haze of the first-stage film and holographic gratings recorded at various spacer thicknesses. The material is composed of a 0.5:1 thiol/alkene functional group ratio with 3 wt % TPO-irradiated first-stage cure for 40 s at 10 mW/cm^2 between two glass plates. The writing stage was achieved with a laser beam of an average intensity of 14 mW/cm^2 for 25 s.

the figure, all haze values of holographic gratings (i.e., stage 2) in films with a thickness from 25 to 100 μm were extremely low and closely resembled the haze of the initial film. This behavior suggests that the holographic recording produced gratings with functionally no haze. However, a distinct increase in haze from 0.3 to 0.8% was observed in the 250 μm films, a phenomenon attributed to phase separation in holographic gratings. The difference in the behavior of the 250 μm films is primarily attributed to the increased path length that incident light has to travel within the film. This longer distance significantly increases the probability of incident light being scattered by domains, while the degree of phase separation remains relatively constant. Furthermore, light attenuation during holographic recording might account for higher haze in thick films. The attenuation of light causes a much lower light intensity in the lower regions of films, which significantly reduces the reaction rate, potentially causing a higher degree of phase separation and consequently higher haze. Nevertheless, it is still noteworthy to achieve a remarkably low haze value of 0.8% in the 250 μm thick film and is of great interest for applications in high optical quality holographic elements. This exceptional reduction of haze is largely attributed to the covalent incorporation of reactive groups (disulfides and alkenes) in the initial-stage network and the formation of an integrated network during the holographic recording. This integration significantly restricts any significant phase separation during the recording, contributing to the minimal haze observed.

CONCLUSIONS

A two-stage photopolymer system was investigated utilizing thiol−ene- and disulfide−ene-based chemistries for fabricating materials with changes in mechanical, chemical, and optical properties. Semiorthogonality between the thiol−ene and disulfide−ene chemistries was employed to establish a two-stage system by utilizing the difference in the reaction rates between the two stages. The second-stage disulfide−ene reaction comprises sequential disulfide cleavage and thioether formation, which enables both significant modulus increase and dynamic cross-linking. Due to the distinctive combination of these two features, the two-stage system was shown to have remarkable shape fixation capability and control over localized stress in the second-stage disulfidation. Additionally, extremely low haze holographic gratings were recorded in the two-stage system because of the nature of having minimal freely diffusing monomers in the system. In this system, almost all functional groups capable of reacting in the second stage are tethered to the initial matrix, therefore immobilizing the writing components prior to the disulfide−ene holographic recording. We believe that a wide variety of applications based on two-stage photopolymers could benefit from having these considerations in their materials design.

EXPERIMENTAL SECTION

Synthesis of DSDVE. Monomers were prepared as previously described.[26] Briefly, to dithiodiglycolic acid (1 equiv, dissolved in anhydrous THF at approximately 0.1 M) was added 1,4-butanediol vinyl ether (3 equiv) followed by diisopropylcarbodiimide (2.5 equiv) and 4-dimethylaminopyridine (0.15 equiv). After stirring at room temperature for 72 h, the reaction was filtered through Celite and washed with additional THF. The filtrate was concentrated in vacuo and purified by column chromatography (100% DCM), yielding a pure product as a clear light-yellow oil (∼70% yield).

Reaction Kinetics. A Fourier transform infrared (FTIR) spectrometer (Nicolet 8700) was used to measure kinetics by monitoring the vinyl and thiol peak area change at 1580−1670 and 2520−2620 cm^{-1}, respectively. The conversion was calculated as the ratio of the real-time peak area to the peak area of initial spectra.

Photorheology. The shear storage modulus of mixtures was determined by using a rheometer (Ares, TA) at a constant shear rate. The strain and frequency were set to be 0.5% and 1 Hz, respectively. A 405 nm LED lamp was used as the light source. In every test, the light was turned on after 30 s equilibration at the targeted shear rate.

Refractive Index Measurement. The refractive index of the samples was measured using an Abbe refractometer. First- and second-stage films were photopolymerized directly in a sample holder, and the measurement was done right after the polymerization.

Photolithography. An initial first-stage film was prepared by mixing DSDVE and PETMP (0.5:1 thiol/alkene stoichiometric ratio) with 3 wt % TPO, and then, the mixture was flood-cured between glass plates with 250 μM spacers using 405 nm light at an intensity of 10 mW/cm^2 for 40 s. Later, photomasks were used to selectively initiate the second-stage reaction using 405 nm light with a light intensity of 10 mW/cm^2 for 3 min.

Preparation of First-Stage Films for Holographic Recording. PETMP and DSDVE at a specific ratio were mixed with 3 wt % TPO. The mixture was cast between glass plates with spacers of specific thickness. The sample was irradiated at 405 nm at 10 mW/cm^2 for various times for the first-stage curing.

Haze Measurement. Haze was measured by using a BYK haze-gard haze meter. Films sandwiched between two glass slides were used directly for haze measurements after holographic recording.

Holographic Recording. A transmission hologram was recorded in a two-beam interference setup using a 405 nm laser diode (Ondax, 40 mW) with a maximum total light intensity of 16 mW/cm^2. Grating periods of 1 μm were used in our experiments, which were realized by

https://doi.org/10.1021/acs.macromol.3c01728
Macromolecules 2023, 56, 9778−9786

recording at external recording half angles of 11.2°. Besides, hologram developments during the recording process were probed simultaneously via a 633 nm He−Ne laser (Thorlabs) aligned approximately at the Bragg reconstruction angle. After writing, a sample rotation from −8 to 8° at a speed of 0.3°/s was applied to obtain the angular selectivity of holographic gratings.

AUTHOR INFORMATION

Corresponding Author

Christopher N. Bowman − *Department of Chemical and Biological Engineering and Materials Science and Engineering Program, University of Colorado Boulder, Boulder, Colorado 80303, United States;* orcid.org/0000-0001-8458-7723; Email: christopher.bowman@colorado.edu

Authors

Yunfeng Hu − *Department of Chemistry, University of Colorado Boulder, Boulder, Colorado 80303, United States;* orcid.org/0000-0001-6230-9941

Shafer M. Soars − *Department of Chemistry, University of Colorado Boulder, Boulder, Colorado 80303, United States*

Bruce E. Kirkpatrick − *Department of Chemical and Biological Engineering and The BioFrontiers Institute, University of Colorado Boulder, Boulder, Colorado 80303, United States; Medical Scientist Training Program, University of Colorado Anschutz Medical Campus, Aurora, Colorado 80045, United States*

Maciej Podgorski − *Department of Chemical and Biological Engineering, University of Colorado Boulder, Boulder, Colorado 80303, United States; Department of Polymer Chemistry, Institute of Chemical Sciences, Faculty of Chemistry, Maria Curie-Sklodowska University, Lublin 20-031, Poland*

Nicholas Bongiardina − *Materials Science and Engineering Program, University of Colorado Boulder, Boulder, Colorado 80303, United States*

Benjamin D. Fairbanks − *Department of Chemical and Biological Engineering, University of Colorado Boulder, Boulder, Colorado 80303, United States*

Kristi S. Anseth − *Department of Chemical and Biological Engineering, The BioFrontiers Institute, and Materials Science and Engineering Program, University of Colorado Boulder, Boulder, Colorado 80303, United States;* orcid.org/0000-0002-5725-5691

Complete contact information is available at: https://pubs.acs.org/10.1021/acs.macromol.3c01728

Author Contributions

The manuscript was written incorporating contributions of all authors. All authors have given approval to the final version of the manuscript.

Notes

The authors declare no competing financial interest.

ACKNOWLEDGMENTS

The authors thank the financial support from NSF (1808484) that made this work possible.

REFERENCES

(1) Paruli, E., III; Soppera, O.; Haupt, K.; Gonzato, C. Photopolymerization and Photostructuring of Molecularly Imprinted Polymers. *ACS Appl. Polym. Mater.* **2021**, *3* (10), 4769−4790.

(2) Xu, X.; Awad, A.; Robles-Martinez, P.; Gaisford, S.; Goyanes, A.; Basit, A. W. Vat photopolymerization 3D printing for advanced drug delivery and medical device applications. *J. Controlled Release* **2021**, *329*, 743−757.

(3) Li, X.; Gai, Y.; Sun, M.; Li, Y.; Xu, S. Drum Tower-Inspired Kirigami Structures for Rapid Fabrication of Multifunctional Shape-Memory Smart Devices with Complex and Rigid 3D Geometry in a Two-Stage Photopolymer. *Adv. Funct. Mater.* **2022**, *32* (40), No. 2205842, DOI: 10.1002/adfm.202205842.

(4) Pagac, M.; Hajnys, J.; Ma, Q.-P.; Jancar, L.; Jansa, J.; Stefek, P.; Mesicek, J. A Review of Vat Photopolymerization Technology: Materials, Applications, Challenges, and Future Trends of 3D Printing. *Polymers* **2021**, *13* (4), No. 598, DOI: 10.3390/polym13040598.

(5) Lawrence, J.; O'Neill, F.; Sheridan, J. Photopolymer holographic recording material. *Optik* **2001**, *112* (10), 449−463.

(6) Corrigan, N.; Boyer, C. 100th Anniversary of Macromolecular Science Viewpoint: Photochemical Reaction Orthogonality in Modern Macromolecular Science. *ACS Macro Lett.* **2019**, *8* (7), 812−818.

(7) Cox, C. A.; Ogorek, A. N.; Habumugisha, J. P.; Martell, J. D. Switchable DNA Photocatalysts for Radical Polymerization Controlled by Chemical Stimuli. *J. Am. Chem. Soc.* **2023**, *145* (3), 1818−1825.

(8) Stansbury, J. W. Curing dental resins and composites by photopolymerization. *J. Esthetic Restor. Dent.* **2000**, *12* (6), 300−308, DOI: 10.1111/j.1708-8240.2000.tb00239.x.

(9) Photopolymerization *Polymers and Light* 2007, pp 273−304.

(10) Zhang, X.; Xi, W.; Huang, S.; Long, K.; Bowman, C. N. Wavelength-Selective Sequential Polymer Network Formation Controlled with a Two-Color Responsive Initiation System. *Macromolecules* **2017**, *50* (15), 5652−5660.

(11) Kuang, X.; Zhao, Z.; Chen, K.; Fang, D.; Kang, G.; Qi, H. J. High-speed 3D printing of high-performance thermosetting polymers via two-stage curing. *Macromol. Rapid Commun.* **2018**, *39* (7), No. 1700809, DOI: 10.1002/marc.201700809.

(12) Glugla, D. J.; Alim, M. D.; Byars, K. D.; Nair, D. P.; Bowman, C. N.; Maute, K. K.; McLeod, R. R. Rigid origami via optical programming and deferred self-folding of a two-stage photopolymer. *ACS Appl. Mater. Interfaces* **2016**, *8* (43), 29658−29667.

(13) Zhang, B.; Serjouei, A.; Zhang, Y.-F.; Wu, J.; Li, H.; Wang, D.; Low, H. Y.; Ge, Q. Dual-stage thermosetting photopolymers for advanced manufacturing. *Chem. Eng. J.* **2021**, *411*, No. 128466, DOI: 10.1016/j.cej.2021.128466.

(14) Hergert, J. E.; Glugla, D. J.; Sullivan, A. C.; Alim, M. D.; McLeod, R. R. High efficiency Fresnel lens design and fabrication in a two-stage photopolymer. *Opt. Lett.* **2019**, *44* (7), 1540−1543.

(15) Alim, M. D.; Glugla, D. J.; Mavila, S.; Wang, C.; Nystrom, P. D.; Sullivan, A. C.; McLeod, R. R.; Bowman, C. N. High Dynamic Range (Δ n) Two-Stage Photopolymers via Enhanced Solubility of a High Refractive Index Acrylate Writing Monomer. *ACS Appl. Mater. Interfaces* **2018**, *10* (1), 1217−1224.

(16) Podgórski, M.; Nair, D. P.; Chatani, S.; Berg, G.; Bowman, C. N. Programmable Mechanically Assisted Geometric Deformations of Glassy Two-Stage Reactive Polymeric Materials. *ACS Appl. Mater. Interfaces* **2014**, *6* (9), 6111−6119.

(17) Cox, L. M.; Martinez, A. M.; Blevins, A. K.; Sowan, N.; Ding, Y.; Bowman, C. N. Nanoimprint lithography: Emergent materials and methods of actuation. *Nano Today* **2020**, *31*, No. 100838.

(18) Nair, D. P.; Cramer, N. B.; Gaipa, J. C.; McBride, M. K.; Matherly, E. M.; McLeod, R. R.; Shandas, R.; Bowman, C. N. Two-Stage Reactive Polymer Network Forming Systems. *Adv. Funct. Mater.* **2012**, *22* (7), 1502−1510.

(19) Guo, B.; Wang, M.; Zhang, D.; Sun, M.; Bi, Y.; Zhao, Y. High Refractive Index Monomers for Improving the Holographic Recording Performance of Two-Stage Photopolymers. *ACS Appl. Mater. Interfaces* **2023**, *15* (20), 24827−24835.

(20) Kowalski, B. A.; McLeod, R. R. Design concepts for diffusive holographic photopolymers. *J. Polym. Sci., Part B: Polym. Phys.* **2016**, *54* (11), 1021−1035.
(21) Naydenova, I.; Jallapuram, R.; Howard, R.; Martin, S.; Toal, V. Investigation of the diffusion processes in a self-processing acrylamide-based photopolymer system. *Appl. Opt.* **2004**, *43* (14), 2900−2905.
(22) Boots, H.; Kloosterboer, J.; Serbutoviez, C.; Touwslager, F. Polymerization-Induced Phase Separation. 1. Conversion− Phase Diagrams. *Macromolecules* **1996**, *29* (24), 7683−7689.
(23) Murata, K.; Sachin, J.; Etori, H.; Anazawa, T. Photopolymerization-induced phase separation in binary blends of photocurable/linear polymers. *Polymer* **2002**, *43* (9), 2845−2859.
(24) Hu, Y.; Kowalski, B. A.; Mavila, S.; Podgórski, M.; Sinha, J.; Sullivan, A. C.; McLeod, R. R.; Bowman, C. N. Holographic Photopolymer Material with High Dynamic Range (Δ n) via Thiol−Ene Click Chemistry. *ACS Appl. Mater. Interfaces* **2020**, *12* (39), 44103−44109.
(25) Hu, Y.; Mavila, S.; Podgórski, M.; Kowalski, J. E.; McLeod, R. R.; Bowman, C. N. Manipulating the Relative Rates of Reaction and Diffusion in a Holographic Photopolymer Based on Thiol−Ene Chemistry. *Macromolecules* **2022**, *55*, 1822−1833, DOI: 10.1021/acs.macromol.1c02528.
(26) Soars, S. M.; Bongiardina, N. J.; Fairbanks, B. D.; Podgórski, M.; Bowman, C. N. Spatial and Temporal Control of Photomediated Disulfide−Ene and Thiol−Ene Chemistries for Two-Stage Polymerizations. *Macromolecules* **2022**, *55* (5), 1811−1821.
(27) Bongiardina, N. J.; Soars, S. M.; Podgorski, M.; Bowman, C. N. Radical-disulfide exchange in thiol−ene−disulfidation polymerizations. *Polym. Chem.* **2022**, *13* (27), 3991−4003.
(28) Nelson, B. R.; Kirkpatrick, B. E.; Miksch, C. E.; Davidson, M. D.; Skillin, N. P.; Hach, G. K.; Khang, A.; Hummel, S. N.; Fairbanks, B. D.; Burdick, J. A.; Bowman, C. N.; Anseth, K. S. Photoinduced Dithiolane Crosslinking for Multiresponsive Dynamic Hydrogels *Adv. Mater., n/a* n/a 2211209 DOI: 10.1002/adma.202211209.
(29) Zheng, N.; Xu, Y.; Zhao, Q.; Xie, T. Dynamic Covalent Polymer Networks: A Molecular Platform for Designing Functions beyond Chemical Recycling and Self-Healing. *Chem. Rev.* **2021**, *121* (3), 1716−1745.
(30) Hammer, L.; Van Zee, N. J.; Nicolaÿ, R. Dually Crosslinked Polymer Networks Incorporating Dynamic Covalent Bonds. *Polymers* **2021**, *13* (3), 396.
(31) Saed, M. O.; Terentjev, E. M. Siloxane crosslinks with dynamic bond exchange enable shape programming in liquid-crystalline elastomers. *Sci. Rep.* **2020**, *10* (1), No. 6609, DOI: 10.1038/s41598-020-63508-4.
(32) Khan, A.; Stucky, G. D.; Hawker, C. J. High-Performance, Nondiffusive Crosslinked Polymers for Holographic Data Storage. *Adv. Mater.* **2008**, *20* (20), 3937−3941.
(33) Kim, K.; Lim, Y.; Son, H.; Hong, S. J.; Shin, C.-W.; Baek, D.; Kim, H. H.; Kim, N.; Bang, J.; Lee, S. Optical Fourier Volumes: A Revisiting of Holographic Photopolymers and Photoaddressable Polymers. *Adv. Opt. Mater.* **2022**, *10* (23), No. 2201421, DOI: 10.1002/adom.202201421.
(34) Xiong, J.; Yin, K.; Li, K.; Wu, S.-T. Holographic optical elements for augmented reality: principles, present status, and future perspectives. *Adv. Photonics Res.* **2021**, *2* (1), No. 2000049, DOI: 10.1002/adpr.202000049.

https://doi.org/10.1021/acs.macromol.3c01728
Macromolecules 2023, 56, 9778−9786